Water Supply

IWA PUBLISHING

Water Supply Vol 00 No 0, 1 doi: 10.2166/ws.2021.184

Adsorption of nitrate and nitrite from aqueous solution by magnetic Mg/Fe hydrotalcite

Jing Chen[a], Yawei Wei[b], Haoyu Ji[a], Pengliang Guo[a], Dongjin Wan[b,*], Bo Li[a] and Xuzhuo Sun[a]
[a] School of Chemistry and Chemical Engineering, Henan University of Technology, Zhengzhou 450001, China
[b] School of Environmental Engineering, Henan University of Technology, Zhengzhou 450001, China
*Corresponding author. E-mail: djwan@haut.edu.cn

DW, 0000-0003-4656-5544

ABSTRACT

In this study, magnetic Mg/Fe hydrotalcite calcined material (M-CHT) was synthesized through the co-precipitation and calcination method, and was used to effectively remove nitrate and nitrite from water. M-CHT can restore its original layered structure after the adsorption of nitrate or nitrite, and can be easily separated by an applied magnetic field. The first-order and pseudo-second-order kinetic models ($R^2 \geq 0.97$) can better describe the adsorption kinetic process. The equilibrium isotherm showed that the Langmuir model provided a better fit to the experimental data than the Freundlich model for nitrates and nitrites. With temperature increased from 298 to 308 K, the maximum adsorption capacity obtained by the Langmuir model increased from 10.60 to 16.90 mg-N/g for nitrate and 7.89 to 14.28 mg-N/g for nitrite, respectively. The adverse effect of coexisting anions ranked in the order of $ClO_4^- > Cl^- > SO_4^{2-} > F^- > CO_3^{2-} > PO_4^{3-}$. The actual Fe^{2+}/Fe^{3+} value of M-CHT (0.56) is nearly consistent with the theoretical value of 0.5, and the saturation magnetic strength value of M-CHT is 9.15 emu/g, greatly contributing to the solid–liquid separation. Overall, M-CHT with features of magnetic properties and satisfactory adsorption capacity exhibits great promise for application in wastewater purification.

Key words: adsorption, hydrotalcite, isotherm, kinetics, nitrate and nitrite

HIGHLIGHTS

- Magnetic Mg/Fe hydrotalcite was synthesized by the co-precipitation method.
- Magnetic Mg/Fe hydrotalcite subjected to calcination at 500 °C (M-CHT) recovered its original double layer after the adsorption of nitrate and nitrite.
- The adsorption capacity was 16.90 mg-N/g for nitrate and 14.28 mg-N/g for nitrite at 35 °C.

GRAPHICAL ABSTRACT

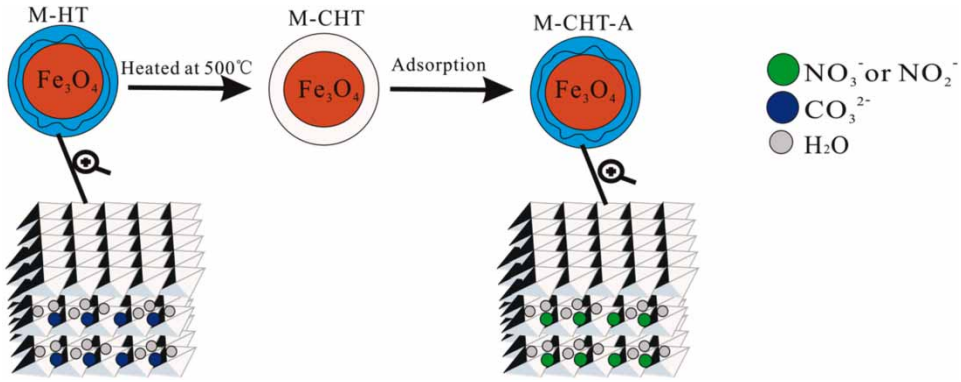

INTRODUCTION

Since the 1960s, with the development of industry and agriculture, several countries have experienced different degrees of groundwater pollution from nitrate (Galloway *et al.* 2008). Nitrates in high concentrations and their

reduction to nitrites result in an adverse effect on the environment, and could potentially cause human health problems such as blue baby syndrome in infants and stomach cancer in adults (Majumdar & Gupta 2000; Kim-Shapiro *et al.* 2005; Boehm 2019). Excess of nitrate in drinking water can also lead to various types of cancer in humans (Aliaskari & Schäfer 2020).

Several methods for removal of nitrate or nitrite from water have been applied, such as reverse osmosis (Berkani *et al.* 2019), catalytic reduction (Han *et al.* 2019; Elias *et al.* 2020), biological denitrification (Mulholland *et al.* 2008; Liu *et al.* 2021a), ion exchange and electrodialysis (Wiercik *et al.* 2020; Zeng *et al.* 2020). However, biological processes are easily affected by temperature, and the effluent needs further treatment, such as disinfection (Chen *et al.* 2009; Zeng *et al.* 2020). Reverse osmosis and electrodialysis are relatively expensive, and merely displace nitrate or nitrite into the concentrated waste brine, causing disposal problems (Samatya *et al.* 2006). Ion exchange needs high energy or a high or expensive dose of the reagent (Zeng *et al.* 2020). In recent decades, adsorption methods have received great attention in the removal of nitrate or nitrite from water, due to their simplicity, sludge-free operation, ease of handling and the availability of various adsorbents (Song *et al.* 2016; Nassar *et al.* 2020). So far, clay materials such as hydrotalcites, with the advantages of low cost, abundant sources and easy preparation, have gained great attention from researchers. Hydrotalcite comprises up and down parallel layers and a large internal space for exchange of anions from water (Jung *et al.* 2020). Carbonate ions and crystal water are present in the interlayer (Saifullah & Hussein 2015). Upper and lower surfaces typically include metal oxide and metal hydroxide (Xia *et al.* 2020). The layer structure exhibits positive charge, and the internal anion exhibits negative charge, eventually rendering the hydrotalcite electrically neutral (Li *et al.* 2020). Hydrotalcite possesses a unique microporous structure, tunable denaturation, memory effect of calcination, interlayer anion-exchange ability, and a high degree of order (Ogata *et al.* 2018; Cheng *et al.* 2021). In a study reported previously by our group, calcined Mg/Al hydrotalcite possessed a high adsorption capacity for nitrate (34.36 mg N/g) and nitrite (37.17 mg N/g) (Wan *et al.* 2012). However, issues related to the effective separation and recovery of hydrotalcite from solution still need to be resolved. The preparation of magnetic hydrotalcite has been developed to resolve the above-mentioned problem, and it has been applied to adsorb toxic anions or compounds such as methyl orange (Deng *et al.* 2016), phosphate (Sun *et al.* 2013) and arsenic (Toledo *et al.* 2010). However, as far as we know, research on the adsorption properties of magnetic hydrotalcite for nitrate and nitrite is still limited.

Considering that Al can damage the human body and has negative effects on health, in this study, magnetic Mg/Fe hydrotalcite calcined material (M-CHT) was synthesized through the co-precipitation and calcination method, and then was used to remove nitrate and nitrite from water. The adsorption properties (including kinetics and isotherm) for nitrate and nitrite over M-CHT under batch conditions were investigated. Moreover, the adsorption mechanism was also analyzed based on characterization (XRD, XPS, FTIR and VSM).

MATERIALS AND METHODS

Materials

$FeCl_3{\cdot}6H_2O$, $MgCl_2{\cdot}6H_2O$, $FeCl_2{\cdot}4H_2O$, $NaNO_2$, $NaNO_3$, NaOH and Na_2CO_3 were all of analytical grade and purchased from Kemiou Chemical Reagent Co., Ltd. (Tianjin, China). The solutions used in all experiments were prepared using ultrapure water of 18.25 MΩ. The 20% ammonia used was in the form of ammonium solution.

Synthesis of M-HT and M-CHT

M-HT was synthesized by the co-precipitation method. First, a magnetic matrix solution was prepared by dissolution of $FeCl_2{\cdot}4H_2O$ (0.24 mol/L Fe^{2+}) and $FeCl_3{\cdot}6H_2O$ (0.48 mol/L Fe^{3+}) in 100 mL deionized (DI) water. Under the conditions of a controlled temperature of 45 ± 1 °C and vigorous stirring, 20% ammonia solution was added dropwise into the above solution to adjust the pH at 11 ± 1. The resulting precipitate was aged at 45 ± 1 °C for 30 min. The as-obtained oily black precipitate was centrifuged and washed with the deionized water several times until the solution pH was neutral. The obtained substance was stored in a 500 mL conical flask containing 100 mL of deionized water for further use.

Next, $MgCl_2{\cdot}6H_2O$ (1.2 mol/L) and $FeCl_3{\cdot}6H_2O$ (0.4 mol/L) were dissolved in 200 mL of deionized water (solution A). Then, solution B containing a mixture of 25.60 g of NaOH (3.2 mol/L) and 4.24 g of Na_2CO_3 (0.2 mol/L) was prepared. The two solutions (A and B) were simultaneously added dropwise into 100 mL of the as-prepared magnetic matrix water under vigorous stirring. The temperature and pH were maintained constant at 40 ± 1 °C

and 10 ± 1, respectively. The resulting slurry was stirred for 2 h and added into a thermostatic water bath at 65 ± 1 °C for ~18 h. The resulting product was centrifuged and washed with the deionized water several times until the electrical conductivity of the supernatant was less than 300 μs/cm. Then, the product was dried at 70 °C and sieved with 100 mesh to obtain the powder, which was marked as M-HT. M-HT was subjected to calcination at 500 °C for 5 h, and sieved with 100 mesh to obtain the final product, which was marked as M-CHT.

Adsorption kinetics study

The adsorption capacity studies for nitrate or nitrite by M-CHT were conducted in a 500 mL flask in batch mode. The initial nitrate or nitrite concentration was maintained constant at 20 mg N/L. The effect of different temperatures (298, 303 and 308 K) on the adsorption of nitrate or nitrite by M-CHT was investigated. The solution volume and adsorbent dosage were 500 mL and 2 g/L, respectively. The adsorption capacity of M-CHT was calculated by the following equation:

$$q_t = (C_0 - C_t)V/m \tag{1}$$

In this equation, q_t is the adsorbent capacity of the adsorbent at time t, C_0 and C_t (mg N/L) are the initial concentration of nitrate or nitrite and the concentration at time t, respectively, and m is the mass of adsorbent (g).

Adsorption equilibrium study

Adsorption equilibrium studies were carried out by utilizing a constant mass (0.10 g) of M-CHT with 100 mL of the nitrate or nitrite solution. Nitrate or nitrite concentrations were 5, 10, 15, 20, 30, 45, and 60 mg N/L. M-CHT with the nitrate or nitrite solution was placed in a temperature-controlled orbital shaker with a stirring speed of 150 rpm. The pH of the mixture was not adjusted to avoid the effect of other anions. After shaking the flasks for 24 h, the solution sample was filtered by a 0.45 μm membrane. The adsorption capacity of M-CHT toward nitrate or nitrite at equilibrium is denoted as q_e (mg N/g).

Analysis methods

Nitrate and nitrite concentrations were measured by Hitachi U-3010 spectrophotometer. XRD data were recorded in a 2θ range of 5° to 80° on a D8 Advance diffractometer using Cu Kα radiation. X-ray photoelectron spectroscopy (XPS) was measured on a Thermo Scientific Escalab 250SXi. Transmission electron microscopy (TEM) was measured on a Tecnai G2F30 microscope. Fourier transform infrared (FTIR) spectra were measured through a WQF-510 spectrometer.

RESULTS AND DISCUSSION

Kinetics study

As seen in Figure 1, in the first 500 min, M-CHT rapidly adsorbed nitrate and nitrite; then, the adsorption rate became sluggish, and the adsorption saturation time was 750 min. A majority of active adsorption sites were available for nitrite or nitrate in the first 500 min, while after that, the active adsorption sites on M-CHT were gradually saturated. With the contact time increasing, the amount of adsorbed nitrate and nitrite increased, and at 308 K, almost 80% of the nitrate and nitrite was removed in 750 min.

With the temperature increasing from 298 to 308 K, the adsorption rates of nitrate and nitrite increased. Three common kinetics models including first-order, pseudo-second-order and intraparticle diffusion kinetics models were used to fit the experimental data, which are expressed by the following equations (Allen *et al.* 1989; Ho & Mckay 1998; Ogata *et al.* 2018):

$$\text{First-order equation: } \ln(q_e - q_t) = \ln q_e - k_1 t \tag{2}$$

$$\text{Pseudo-second-order equation: } \frac{t}{q_t} = \frac{1}{k_2 q_e^2} + \frac{t}{q_e} \tag{3}$$

$$\text{Intraparticle diffusion equation: } q_t = k_3 t^{0.5} \tag{4}$$

where q_e and q_t are the adsorption amounts of nitrite or nitrate at equilibrium and at time t (min), respectively, k_1 is the first-order reaction rate constant (min^{-1}), t (time) is reaction time, and k_2 (g/mg min) and

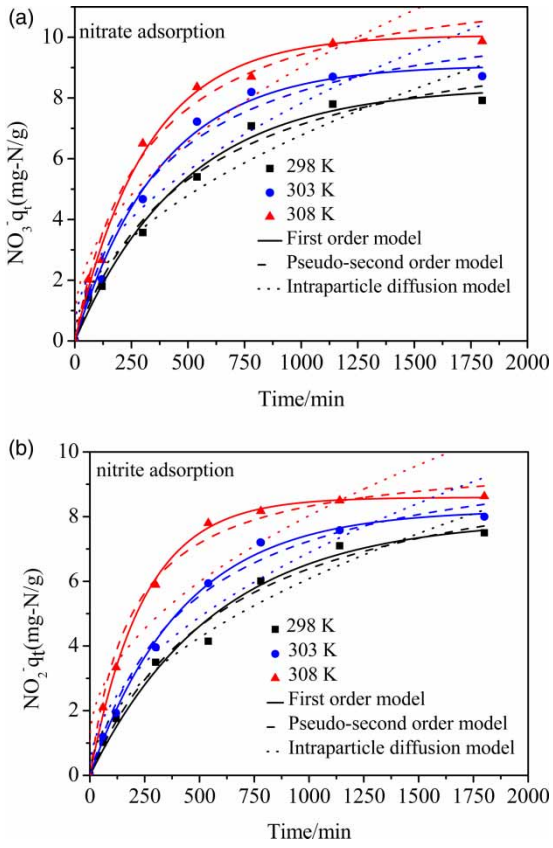

Figure 1 | Adsorption kinetics of (a) nitrate and (b) nitrite by M-CHT at 298, 303, and 308 K. (Solution volume and adsorbent dosage were 500 mL and 2 g/L, respectively.)

k_3 (mg/g $min^{0.5}$) are the rate constants of the pseudo-second-order and intraparticle diffusion kinetics models, respectively.

Table 1 shows the adsorption kinetics results which were fitted by the first-order, pseudo-second-order, and intraparticle diffusion models. According to the values of the correlation coefficient with nitrate and nitrite, higher R^2 values ($\geq$0.97) were fitted by the first-order and pseudo-second-order models. Specifically, the first-order model is well fitted, indicating that nitrate and nitrite adsorption rates are controlled by diffusion. In addition, the adsorption data were fitted with the pseudo-second-order model, and adsorption was concluded to be chemical adsorption (Hu *et al.* 2016). In addition, the initial adsorption rate can be calculated by $v_0 = k_2 \times {q_e}^2$ from the pseudo-second-order model. The adsorption rate $v_0(\times 10^{-4})$ of nitrate increased from 209.33 to 404.99 mg/(g·min), while that of nitrite increased from 164.56 to 476.23 mg/(g·min). It can be explained that improving the solution temperature could facilitate the initial adsorption rate of nitrate and nitrite. The adsorption capacities of M-CHT fitted by the first-order model for nitrate at 298, 303 and 308 K were respectively 8.37, 8.11 and 8.78 mg N/g. The corresponding values for nitrite were 7.92, 8.21, and 8.59 mg N/g, indicating that the increase of solution temperature can promote the adsorption of nitrate or nitrite on M-CHT, which is consistent with the above v_0 result.

Equilibrium study

The adsorption isotherm is an important way to describe the maximum adsorption capacity of M-CHT for nitrate or nitrite. To discuss the effect of different temperatures, the adsorption equilibrium of nitrate and nitrite on M-CHT was investigated at 298, 303 and 308 K. As shown in Figure 2, the equilibrium concentration of nitrate or nitrite increased, and the equilibrium adsorption capacity was also increased. With the temperature increasing from 298 to 308 K, adsorption equilibrium was achieved more rapidly. The adsorption capacities of nitrate and nitrite were high at high temperatures.

Table 1 | Kinetics parameters and correlation coefficients (R^2) for three kinetics modes

Anion	temperature K	first-order model				pseudo-second order				intraparticle diffusion model			
		$q_{e,cal}$ (mg/g)	$k_1 \times 10^{-2}$ (min^{-1})	R^2	P	$V_0 \times 10^{-4}$ (mg/(g·min))	$q_{e,cal}$ (mg/g)	$k_2 \times 10^{-4}$ (g/mg min)	R^2	P	$k_{0.5}$ (mg/g min^{-1})	R^2	P
NO_3^--N	298	8.37	0.20	0.9896	5.05477×10^{-8}	209.33	11.00	1.73	0.9825	2.43133×10^{-7}	0.2140	0.9477	9.12237×10^{-6}
	303	8.11	0.26	0.9917	2.27789×10^{-8}	298.12	11.46	2.27	0.9775	4.46344×10^{-7}	0.2391	0.8986	3.91332×10^{-5}
	308	8.78	0.32	0.9916	1.84834×10^{-8}	404.99	12.27	2.69	0.9850	1.04629×10^{-7}	0.2656	0.8966	3.29627×10^{-5}
NO_2^--N	298	7.92	0.17	0.9843	1.93840×10^{-7}	164.56	11.00	1.36	0.9847	1.78946×10^{-7}	0.1967	0.9659	1.95582×10^{-6}
	303	8.21	0.23	0.9972	9.28335×10^{-10}	231.99	10.77	2.04	0.9893	5.28961×10^{-8}	0.2153	0.9312	1.34692×10^{-5}
	308	8.59	0.41	0.9983	1.14430×10^{-10}	476.23	10.12	4.65	0.9906	1.81887×10^{-8}	0.2209	0.8604	5.54217×10^{-5}

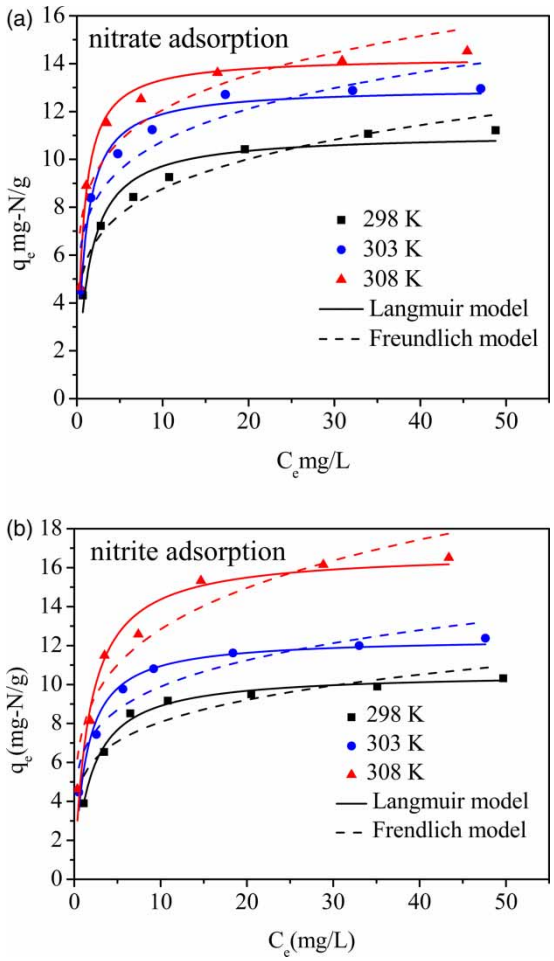

Figure 2 | Adsorption isotherm of (a) nitrate and (b) nitrite on M-CHT at 298, 303 and 308 K. (Solution volume and adsorbent dosage were 100 mL and 1 g/L, respectively.)

Equilibrium data was fitted by two isotherm models: the Langmuir and Freundlich models. These isotherm models are expressed by the following Equations (5) and (6), respectively:

$$Langmuir\ model: q_e = \frac{Q_0 K_L C_e}{1 + K_L C_e} \tag{5}$$

$$Freundlich\ model: q_e = K_F C_e^{1/n} \tag{6}$$

where C_e is the nitrate or nitrite concentration of the solution at equilibrium (mg/L), Q_0 is the monolayer capacity of adsorbent (mg/g), K_L is the Langmuir constant (L/mg), and K_F (mg/g) (L/mg) and n are the Freundlich temperature-dependent constants.

Table 2 summarizes the adsorption isotherm parameters for nitrate and nitrite. The Langmuir isotherm model afforded the better fitting results with R^2 values ($\geq$0.97), which was greater than those obtained by the Freundlich model, indicating that nitrate and nitrite are uniform on the adsorbent surface and adsorption may be monolayer adsorption (Wan *et al.* 2012; Rodrigues *et al.* 2019). Meanwhile, at 298, 303 and 308 K, the maximum adsorption capacities of M-CHT for nitrate were 7.89, 13.00, and 14.28 mg N/g, respectively. The corresponding values for nitrite were 10.60, 12.40 and 16.90 mg N/g. The adsorption capacities of nitrate and nitrite at different temperatures increased, ranking in the order of 298 K < 303 K < 308 K. High temperature was favorable for adsorption; this tendency was in agreement with that reported by Rodrigues *et al.* (2019). At 308 K, M-CHT exhibited highest adsorption capacity, and the Langmuir parameters for nitrate adsorption were $Q_0 = 14.28$ mg N/g, and $K_L =$ 1.39 L/mg; the corresponding values for nitrite were $Q_0 = 16.90$ mg N/g, and $K_L = 0.59$ L/mg.

Table 2 | Adsorption isotherm parameters at different temperatures

	Langmuir: $q_e = \frac{Q_0 K_L C_e}{1 + K_L C_e}$				Freundlich: $q_e = K_F C_e^{1/n}$			
Temperature (K)	Q_0 (mg/g)	K_L (L/mg)	R^2	P	K_F (mg/g)(L/mg)^n	n	R^2	P
NO_3^--N								
298	7.89	0.71	0.9445	8.58917×10^{-7}	5.66	5.25	0.9389	1.08977×10^{-6}
303	13.00	1.07	0.9785	1.06430×10^{-7}	7.25	5.84	0.8620	1.09662×10^{-5}
308	14.28	1.39	0.9892	2.32829×10^{-8}	8.27	6.09	0.8451	1.79982×10^{-5}
NO_2^--N								
298	10.60	0.52	0.9887	1.55678×10^{-8}	5.21	5.26	0.8205	1.53498×10^{-5}
303	12.40	0.75	0.9621	4.28136×10^{-7}	6.45	5.39	0.8869	6.51297×10^{-6}
308	16.90	0.59	0.9542	1.85506×10^{-6}	7.72	7.75	0.9152	8.61090×10^{-6}

The thermodynamic parameters of the adsorption process include the standard free energy change ($\Delta G°$, kJ/mol), the standard enthalpy change ($\Delta H°$, kJ/mol) and the standard entropy change ($\Delta S°$, J/mol·K^{-1}), respectively, which can be calculated by the following equations (Aksu 2002; Debnath & Ghosh 2008):

$$\Delta G^\circ = -RT\ln K_c' \tag{7}$$

$$\ln K_c' = \frac{C_{ad,e}}{C_e} \tag{8}$$

$$\ln K_c' = -\frac{\Delta H^\circ}{RT} + \frac{\Delta S^\circ}{R} \tag{9}$$

where R (8.314 J/mol K) is the ideal gas constant, T (K) is the temperature, $C_{ad,e}$ is the concentration of nitrate or nitrite on M-CHT at equilibrium (mg-N/L) and K_c' is the apparent equilibrium constant. The value of K_c' in the lowest experimental nitrate or nitrite concentration can be obtained (Chudoba *et al.* 2020). It is known that an adsorption reaction is a spontaneous process when $\Delta G°$ are negative values (Shahwan 2021). Herein, the thermodynamic parameters for the adsorption of nitrate and nitrite by M-CHT are given in Table 3. Specifically, $\Delta G°$ are negative values and decrease with temperature increasing, indicating that the adsorption process of nitrate and nitrite by M-CHT is spontaneous (Golban *et al.* 2019), and the positive values of $\Delta H°$ suggest the endothermic nature of the adsorption of nitrate or nitrite by M-CHT. The positive values of $\Delta S°$ illustrate an increase in the randomness of the adsorption process.

Figure 3 and Table 4 present the Arrhenius equations, considering the satisfactory correlation coefficient values of 0.9934 and 0.9298. The adsorption processes have an adsorption activation energy value of 35.92 kJ/mol for nitrate and that of 67.12 kJ/mol for nitrite onto M-CHT. When the E_a value is lower than 40 kJ/mol, the adsorption type can be considered as a physical adsorption process. When the E_a value is greater than 40 kJ/mol, it suggests chemical adsorption (Bagheri *et al.* 2015). Herein, the E_a value of nitrite adsorption was greater than 40 kJ/mol, indicating the feasibility of the adsorption process being predominantly chemical in nature. The E_a value of nitrate adsorption was lower than 40 kJ/mol, which might be physical adsorption.

Table 3 | Thermodynamic parameters of adsorption of nitrate and nitrite by M-CHT

Materials	Temperature (K)	ln K_c'	ΔG^0 (kJ/mol)	ΔH^0 (kJ/mol)	ΔS^0 (J/mol·K^{-1})
Nitrate	298	1.85	−4.58	58.74	212.68
	303	2.31	−5.83		
	308	2.62	−6.70		
Nitrite	298	1.27	−3.14	96.43	334.71
	303	2.13	−5.37		
	308	2.53	−6.47		

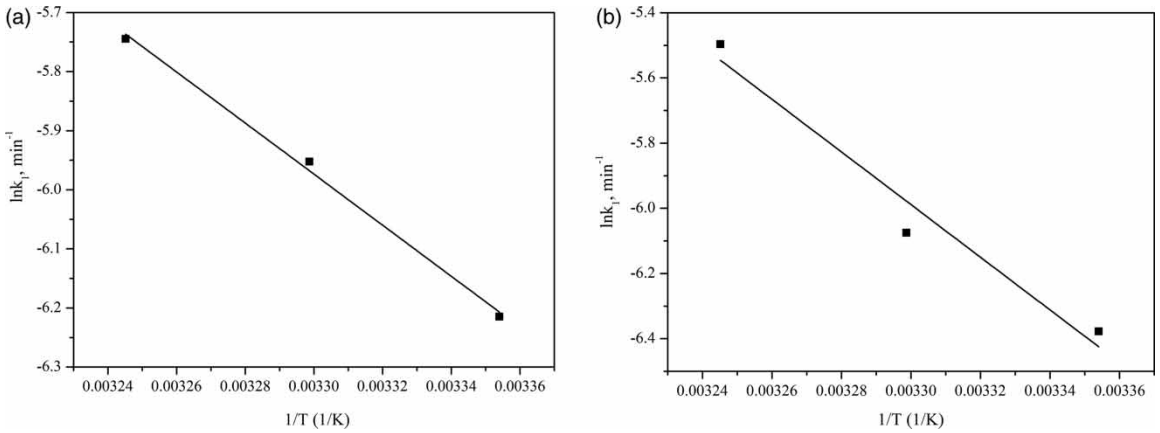

Figure 3 | Arrhenius plots of adsorption of (a) nitrate and (b) nitrite onto M-CHT. (Solution volume and adsorbent dosage were 500 mL and 2 g/L, respectively.)

Table 4 | The energy of activation (E_a) from the Arrhenius plots

	Arrhenius Equation	
Temperature (K)	**E_a (kJ·mol^{-1})**	**R^2**
Nitrate	35.92	0.9934
Nitrite	67.12	0.9298

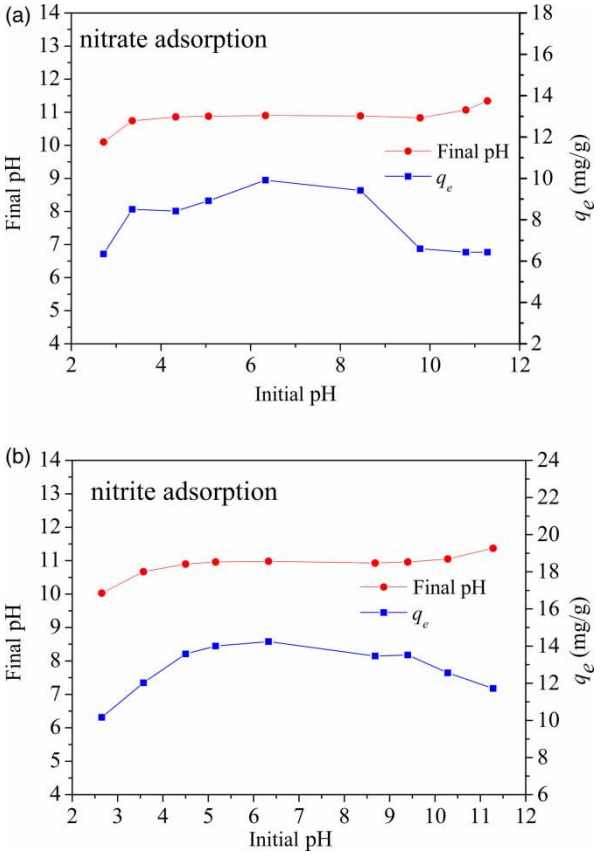

Figure 4 | Effect of the initial pH of the M-CHT solution on the adsorption capacity of (a) nitrate and (b) nitrite, and the final pH value of the solution after adsorption. (Solution volume and adsorbent dosage were 100 mL and 1 g/L, respectively.)

Effects of initial pH

Hydrotalcite-like material is an alkali compound, and the solution pH profoundly affects its adsorption performance. Figure 4 shows the results of adsorption capacities at equilibrium (q_e) under different initial pH values. M-CHT exhibited a high nitrate adsorption capacity at initial pH range of 3.36–8.45, as well as high nitrite adsorption capacity at initial pH range of 3.57–9.4, indicating that M-CHT has a high adsorption capacity toward nitrate and nitrite in a wide range of solution pH. The maximum nitrate and nitrite adsorption capacities were 9.91 mg N/g at pH 6.33 and 14.24 mg N/g at pH 6.38, respectively.

When initial pH was >4.0, the final pH after adsorption exceeded 10.5, suggesting that M-CHT is a strongly alkaline material. After adsorption, pH increased possibly due to the release of OH^- from hydrotalcite. At the same time, at initial pH values of 4–10, these trends were not significant, indicating that hydrotalcite exhibits a certain buffering effect on the change of the solution pH; hence, within a certain range of pH, the effect of pH on the adsorption capacity of nitrate and nitrite by CHT is not extremely significant, and the adoption range is wide (Ahmed *et al.* 2020). With the decrease in the solution pH to 2.50, the nitrate and nitrite adsorption capacities decreased to 6.41 mg N/g and 10.12 mg N/g, respectively, with a corresponding decrease in the final solution pH to 10.09 and 10.04. Thus, a strongly acidic environment reduces the stability of the laminate structure of materials (Ferreira *et al.* 2006), thus decreasing adsorption capacity for anions. With the increase in the pH, the competitive adsorption of nitrate or nitrite by a high number of OH^- in the solution increased, leading to the decreased adsorption of the nitrate or nitrite.

Effects of coexisting anions

Typically, anions such as F^-, Cl^-, ClO_4^-, SO_4^{2-}, CO_3^{2-}, and PO_4^{3-} are present in nitrate- and nitrite-contaminated water, which can compete with nitrate or nitrite for adsorption sites on materials (Gierak & Łazarska 2017). As shown in Figure 5, in the control group (no coexisting ions), the removal efficiencies of nitrate and nitrite by M-CHT were 46.34% and 68.56%, respectively. From the general trend observed in the figure, the adsorption capacity of nitrate and nitrite significantly decreased in the presence of coexisting anions. The order of influence is $PO_4^{3-} > CO_3^{2-} > F^- > SO_4^{2-} > Cl^- > ClO_4^-$. The adsorption ability of M-CHT for nitrite or nitrate from the solution was mainly dependent on the electrical affinity of its positive surface. In the presence of PO_4^{3-} in the solution, the adsorption capacity was significantly decreased. After the calcination of M-CHT, the interlayer water or interlayer anions were lost, and the material surface exhibited a positive charge. The higher the coexisting anion valence, the poorer the adsorption of nitrite or nitrate by M-CHT (Li *et al.* 2016). Thus, PO_4^{3-} is the most competitive anion. In addition, anion radius affected the adsorption capacity. Compared with Cl^-, the anion F^- with smaller radius has the more adverse effect on the adsorption of nitrate or nitrate.

Characterization

XRD analysis

XRD was employed to investigate sample structure. Figure 6 shows the XRD patterns of M-HT, M-CHT, and M-CHT-A. M-CHT-A-NO_3^- and M-CHT-A-NO_2^- represent the calcined hydrotalcite with adsorbed nitrate and nitrite,

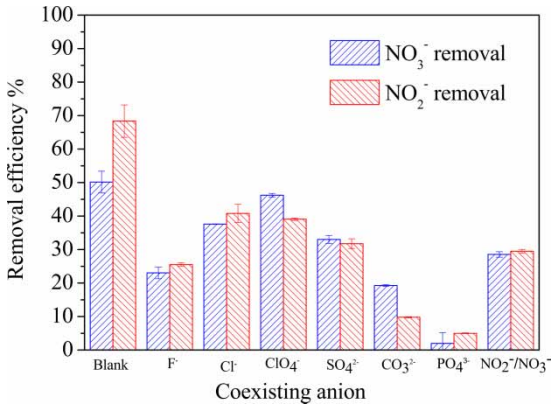

Figure 5 | Effect of coexisting anions on nitrate and nitrite removal by M-CHT. ($T = 25$ °C, pH = 9.08, initial NO_3^--N, NO_2^--N, and coexisting anion concentration was 20 mg/L, M-CHT dosage was 1 g/L, and solution volume was 100 mL.)

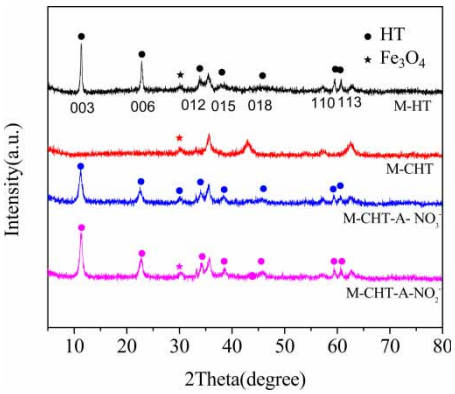

Figure 6 | X-ray diffraction spectra of M-HT, M-CHT, and M-CHT-A.

respectively. As shown in Figure 6, before calcination, M-HT exhibited a typical HT-CO_3^{2-} structure with sharp, symmetric (003), (006), (110) and (113) reflections, as well as wide, symmetric (012), (015) and (018) reflections, revealing the characteristics of the hydrotalcite-like compounds (Wang *et al.* 2018; Kang *et al.* 2020). A peak observed at a 2θ of 30.34° was indexed to Fe_3O_4 (JCPDS 26-1136), indicating that the magnetic substrate had been successfully loaded on the hydrotalcite (Zhang *et al.* 2013). After calcination at 500 °C for 4 h, all of the characteristic reflections (003, 006, 110, 113, 012, 015 and 018) of M-HT disappeared, suggesting the destruction of the layer structure of the M-CHT. Meanwhile, a mixed oxide of Mg(Fe)O with peaks at 43° and 62° (M-CHT) was formed (Yang *et al.* 2012). The peak indexed as Fe_3O_4 can still be clearly observed at 30.34°. Hence, M-CHT should be a mixed metal oxide, and the calcination treatment did not destroy the structure of Fe_3O_4. After adsorption of nitrate or nitrite on M-CHT (M-CHT-A-NO_3^-, M-CHT-A-NO_2^-), the layered structure was reconstructed, which is indicative of the adsorption of nitrate or nitrite on the positive layer and formation of a negative layer.

The interlayer spacing was calculated by using the basal spacing (d003) minus the width of the brucite-like layer (Wan *et al.* 2012). Herein, the internal spaces of CHT and M-CHT were 0.293 nm and 0.299 nm, respectively, indicating that the addition of the magnetic matrix does not affect the internal space of M-HT.

XPS analysis

To analyze the surface composition and elemental states of M-CHT, XPS was adopted. All elements were marked in the full spectrum map (Figure 7(a)). The typical binding energies were observed at 56.92 eV, 301.38 eV, 532.80 eV, and 727.12 eV, corresponding to Mg2p, C1s, O1s, and Fe2p, respectively, which are consistent with the main constituent elements of M-CHT.

As presented in Figure 7(b), the binding energies at 712.3 eV and 725.6 eV were assigned as characteristic of Fe^{3+}, and the binding energies at 710.6 eV and 723.9 eV were assigned as characteristic of Fe^{2+} (Liu *et al.* 2020a). In addition, the binding energy at 719.06 eV is the common satellite peak of both Fe^{3+} and Fe^{2+}. As calculated by the peak areas from XPS, the peak area ratios of Fe^{2+} and Fe^{3+} were 35.96% and 64.04%, respectively. The actual Fe^{2+}/Fe^{3+} value of 0.56 is basically consistent with the theoretical value of 0.5, indicating that Fe_3O_4 is doped in hydrotalcite (Yan *et al.* 2015; Liu *et al.* 2020a).

FTIR analysis

Figure 8 shows FTIR spectra of M-HT, M-CHT and M-CHT-A. The wide band at 3,460 cm^{-1} corresponds to the -OH bending vibration from hydroxyl groups and interlayer water (Yan *et al.* 2015; Shi *et al.* 2020). A weak band at 1,649 cm^{-1} was assigned as the bending vibration of the interlayer water (Abdelkader *et al.* 2011; Liu *et al.* 2020a). The peak at 1,364 cm^{-1} is the vibrational peak of CO_3^{2-} (Saiah *et al.* 2009). The band between 400 cm^{-1} and 800 cm^{-1} is attributed to the stretching bands of the magnesium iron skeleton (Liu *et al.* 2020a). The above results indicate that M-HT exhibits characteristics of hydrotalcite, comprising interlayer water and carbonate, and the introduction of the magnetic substrate does not change its properties.

After calcination, the characteristic peaks of hydrotalcite at 3,460 cm^{-1} and 1,649 cm^{-1} became weak or disappeared, mainly due to the collapse of the lamellar structure, disappearance of functional groups such as OH^-, CO_3^{2-}, and H_2O at high temperature, and conversion of the sample to a mixed oxide (Wan *et al.* 2012). After the adsorption of nitrate or nitrite, new peaks were observed at 1,384 cm^{-1} and 1,271 cm^{-1}, corresponding to nitrate

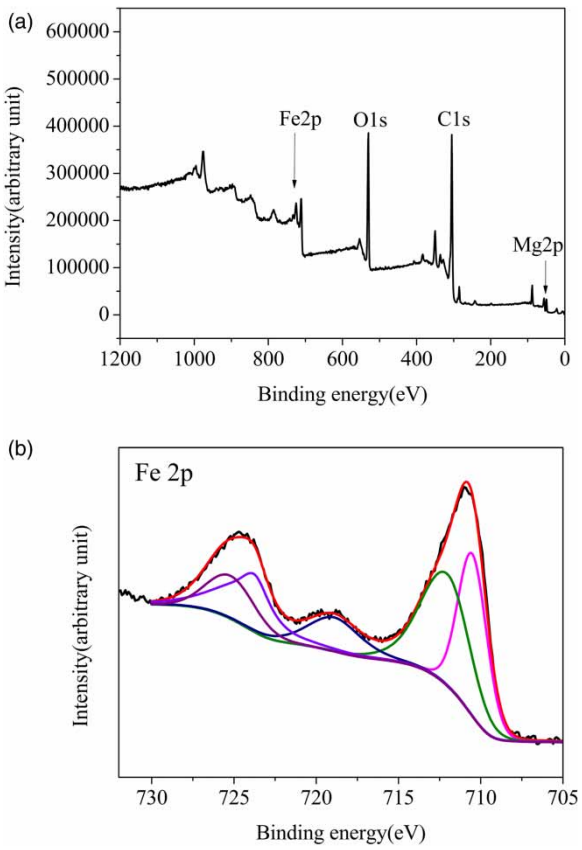

Figure 7 | X-ray photoelectron spectra of M-CHT: (a) full spectrum and (b) Fe2p peaks with the fitting spectrum.

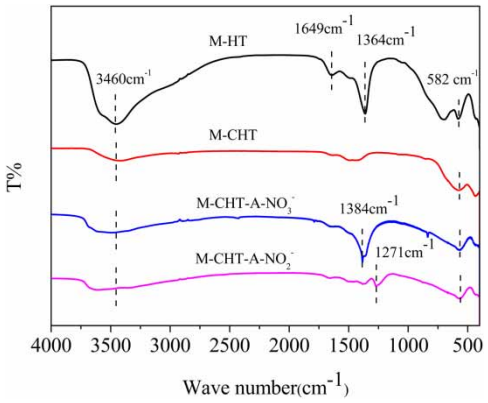

Figure 8 | FTIR spectra of M-HT, M-CHT and M-CHT-A.

and nitrite (Ogata *et al.* 2018), indicating the successful adsorption of nitrate and nitrite on M-CHT. Moreover, for all samples, the peak at 582 cm^{-1} corresponds to the Fe-O stretching vibration (Liu *et al.* 2020b, 2021b), which is a feature of Fe_3O_4 (Pandi & Viswanathan 2016). It indicated that Fe_3O_4 was successfully loaded on the hydrotalcite, and the calcination and adsorption process does not affect the structure of Fe_3O_4.

VSM analysis

XRD, XPS and FTIR results indicated that Fe_3O_4 was successfully loaded on the hydrotalcite matrix. Figure 9 shows the magnetic hysteresis curve of M-CHT at room temperature. M-CHT exhibited a magnetization of 9.15 emu/g. The coercive force and remanence were close to zero, indicating that M-CHT is a superparamagnetic

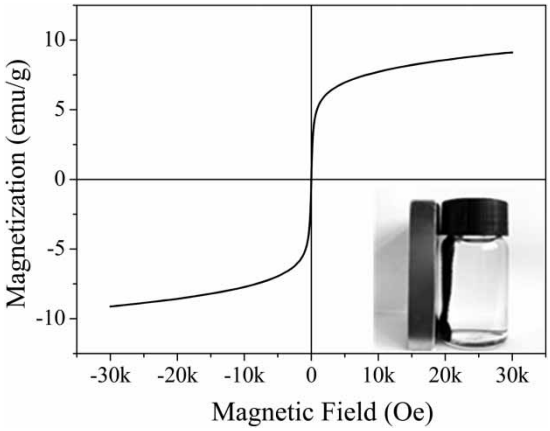

Figure 9 | Magnetization curves of M-CHT.

material (Xu & Wang 2012; Shen *et al.* 2019). The inset image in Figure 9 shows the result of magnetic separation of M-CHT after 5 min, which indicates that M-CHT can be easily separated and recovered.

CONCLUSIONS

In this study, M-CHT synthesized by the co-precipitation and calcination method exhibited high adsorption capacity for nitrate and nitrite from contaminated water under a wide range of pH (initial pH ranged from 3 to 9). The adsorption kinetics and isotherm of nitrate and nitrite can be described with the first-order, pseudo-second-order model and Langmuir model, respectively. In the presence of coexisting anions, the removal efficiency of nitrate and nitrite over M-CHT decreased in the order of $PO_4^{3-} > CO_3^{2-} > F^- > SO_4^{2-} > Cl^- > ClO_4^-$. XRD and FTIR analysis revealed that M-CHT can recover its original layered structure after the adsorption of nitrate or nitrite. Meanwhile, XRD and XPS analysis confirmed that Fe_3O_4 was successfully loaded on hydrotalcite, and did not affect the hydrotalcite structure. M-CHT is a magnetic material and it can be easily recycled using a magnet. Thus, M-CHT exhibits great prospects for application in wastewater purification.

ACKNOWLEDGEMENTS

This work was financially supported by National Natural Science Foundation of China (51878251), Key Scientific and Technological Research Project in Henan Province (192102210170, 14B430005, 182102210398, 172102310137), State Key Laboratory of Materials Processing and Die & Mould Technology, Huazhong University of Science and Technology (P2019-004).

DECLARATION OF INTEREST STATEMENT

The authors declare that they have no known competing financial interests or personal relationships that could have appeared to influence the work reported in this paper.

DATA AVAILABILITY STATEMENT

All relevant data are included in the paper or its Supplementary Information.

REFERENCES

Abdelkader, N. B.-H., Bentouami, A., Derriche, Z., Bettahar, N. & de Ménorval, L.-C. 2011 Synthesis and characterization of Mg–Fe layer double hydroxides and its application on adsorption of Orange G from aqueous solution. *Chemical Engineering Journal* **169**, 231–238.

Ahmed, A., Wang, J., Wang, W., Okonkwo, C. J. & Liu, N. 2020 A practical method to remove perfluorooctanoic acid from aqueous media using layer double hydride system: a prospect for environmental remediation. *Environmental Technology*, doi: 10.1080/09593330.2020.1812733.

Aksu, Z. 2002 Determination of the equilibrium, kinetic and thermodynamic parameters of the batch biosorption of nickel(II) ions onto *Chlorella vulgaris*. *Process Biochemistry* **38**, 89–99.

Aliaskari, M. & Schäfer, A. I. 2020 Nitrate, arsenic and fluoride removal by electrodialysis from brackish groundwater. *Water Research* **190**, 116683.

Allen, S. J., McKay, G. & Khader, K. Y. H. 1989 Intraparticle diffusion of a basic dye during adsorption onto sphagnum peat. *Environmental Pollution* **56**, 39–50.

Bagheri, M., Younesi, H., Hajati, S. & Borghei, S. M. 2015 Application of chitosan–citric acid nanoparticles for removal of chromium (VI). *International Journal of Biological Macromolecules* **80**, 431–444.

Berkani, I., Belkacem, M., Trari, M., Lapicque, F. & Bensadok, K. 2019 Assessment of electrocoagulation based on nitrate removal, for treating and recycling the Saharan groundwater desalination reverse osmosis concentrate for a sustainable management of Albien resource. *Journal of Environmental Chemical Engineering* **7**, 102951.

Boehm, A. B. 2019 Risk-based water quality thresholds for coliphages in surface waters: effect of temperature and contamination aging. *Environmental Science: Processes & Impacts* **21**, 2031–2041.

Chen, L., Li, J. & Ge, M. 2009 Promotional effect of Ce-doped V_2O_5-WO_3/TiO_2 with low vanadium loadings for selective catalytic reduction of NO_x by NH_3. *Journal of Physical Chemistry C* **113**, 21177–21184.

Cheng, J., Zhang, X., Tang, Y., Song, Z. & Jin, X. 2021 Nitrogen removal from domestic wastewater using core-shell anthracite/Mg-layered double hydroxides (LDHs) in constructed wetlands. *Environmental Science and Pollution Research*, doi: 10.1007/s11356-021-13422-7.

Chudoba, D., Łudzik, K., Jażdżewska, M. & Wołoszczuk, S. 2020 Kinetic and equilibrium studies of doxorubicin adsorption onto carbon nanotubes. *International Journal of Molecular Sciences* **21**, 8230.

Debnath, S. & Ghosh, U. C. 2008 Kinetics, isotherm and thermodynamics for Cr(III) and Cr(VI) adsorption from aqueous solutions by crystalline hydrous titanium oxide. *Journal of Chemical Thermodynamics* **40**, 67–77.

Deng, L., Shi, Z., Peng, X. & Zhou, S. 2016 Magnetic calcinated cobalt ferrite/magnesium aluminum hydrotalcite composite for enhanced adsorption of methyl orange. *Journal of Alloys & Compounds* **688**, 101–112.

Elias, W. C., Heck, K. N., Guo, S., Yazdi, S., Ayala-Orozco, C., Grossweiler, S., Domingos, J. B., Ringe, E. & Wong, M. S. 2020 Indium-decorated Pd nanocubes degrade nitrate anions rapidly. *Applied Catalysis B: Environmental* **276**, 119048.

Ferreira, O. P., de Moraes, S. G., Durán, N., Cornejo, L. & Alves, O. L. 2006 Evaluation of boron removal from water by hydrotalcite-like compounds. *Chemosphere* **62**, 80–88.

Galloway, J. N., Townsend, A. R., Erisman, J. W., Bekunda, M., Cai, Z., Freney, J. R., Martinelli, L. A., Seitzinger, S. P. & Sutton, M. A. 2008 Transformation of the nitrogen cycle: recent trends, questions, and potential solutions. *Science* **320**, 889–892.

Gierak, A. & Łazarska, I. 2017 Adsorption of nitrate, nitrite, and ammonium ions on carbon adsorbents. *Adsorption Science & Technology* **35**, 721–727.

Golban, L., Lupa, L., Cocheci, L. & Pode, R. 2019 Synthesis of MgFe layered double hydroxide from iron-containing acidic residual solution and its adsorption performance. *Crystals* **9**, 514.

Han, L., Cai, S., Gao, M., Hasegawa, J.-Y., Wang, P., Zhang, J., Shi, L. & Zhang, D. 2019 Selective catalytic reduction of NO_x with NH_3 by using novel catalysts: state of the art and future prospects. *Chemical Reviews* **119**, 10916–10976.

Ho, Y. S. & McKay, G. 1998 Sorption of dye from aqueous solution by peat. *Chemical Engineering Journal* **70**, 115–124.

Hu, Q. L., Chen, N., Feng, C. P. & Hu, W. W. 2016 Kinetic studies for nitrate adsorption on granular chitosan–Fe(III) complex. *Desalination and Water Treatment* **57**, 27783–27793.

Jung, I.-K., Jo, Y., Han, S.-C. & Yun, J.-I. 2020 Efficient removal of iodide anion from aqueous solution with recyclable core-shell magnetic Fe_3O_4@Mg/Al layered double hydroxide (LDH). *Science of the Total Environment* **705**, 135814.

Kang, J., Levitskaia, T. G., Park, S., Kim, J., Varga, T. & Um, W. 2020 Nanostructured MgFe and CoCr layered double hydroxides for removal and sequestration of iodine anions. *Chemical Engineering Journal* **380**, 122408.

Kim-Shapiro, D. B., Gladwin, M. T., Patel, R. P. & Hogg, N. 2005 The reaction between nitrite and hemoglobin: the role of nitrite in hemoglobin-mediated hypoxic vasodilation. *Journal of Inorganic Biochemistry* **99**, 237–246.

Li, R. H., Wang, J. J., Zhou, B. Y., Awasthi, M. K., Ali, A., Zhang, Z. Q., Gaston, L. A., Lahori, A. H. & Mahar, A. 2016 Enhancing phosphate adsorption by Mg/Al layered double hydroxide functionalized biochar with different Mg/Al ratios. *Science of the Total Environment* **559**, 121–129.

Li, J., Dong, S., Wang, Y., Dou, X. & Hao, H. 2020 Nitrate removal from aqueous solutions by magnetic cationic hydrogel: effect of electrostatic adsorption and mechanism. *Journal of Environmental Sciences* **91**, 177–188.

Liu, Y., Chen, Z., Guo, P., Shi, Y., Chen, J., He, Q. & Wan, D. 2020a Adsorption of high concentration perchlorate from aqueous solution onto Mg/Fe magnetic hydrotalcite calcined product (MAG@CHT): kinetics and isotherm study. *Desalination and Water Treatment* **204**, 328–339.

Liu, Y., Li, J., Wu, L., Shi, Y., He, Q., Chen, J. & Wan, D. 2020b Magnetic spent bleaching earth carbon (Mag-SBE@C) for efficient adsorption of tetracycline hydrochloride: response surface methodology for optimization and mechanism of action. *Science of the Total Environment* **722**, 137817.

Liu, T., Liu, S., He, S., Tian, Z. & Zheng, M. 2021a Minimization of N_2O emission through intermittent aeration in a sequencing batch reactor (SBR): main behavior and mechanism. *Water* **13**, 210.

Liu, Y., Li, J., Wu, L., Wan, D., Shi, Y., He, Q. & Chen, J. 2021b Synergetic adsorption and Fenton-like degradation of tetracycline hydrochloride by magnetic spent bleaching earth carbon: insights into performance and reaction mechanism. *Science of the Total Environment* **761**, 143956.

Majumdar, D. & Gupta, N. 2000 Nitrate pollution of groundwater and associated human health disorders. *Indian Journal of Environmental Health* **42**, 28–39.

Mulholland, P. J., Helton, A. M., Poole, G. C., Hall Jr., R. O., Hamilton, S. K., Peterson, B. J., Tank, J. L., Ashkenas, L. R., Cooper, L. W., Dahm, C. N., Dodds, W. K., Findlay, S. E. G., Gregory, S. V., Grimm, N. B., Johnson, S. L., McDowell, W. H., Meyer, J. L., Valett, H. M., Webster, J. R., Arango, C. P., Beaulieu, J. J., Bernot, M. J., Burgin, A. J., Crenshaw, C. L., Johnson, L. T.,

Niederlehner, B. R., O'Brien, J. M., Potter, J. D., Sheibley, R. W., Sobota, D. J. & Thomas, S. M. 2008 Stream denitrification across biomes and its response to anthropogenic nitrate loading. *Nature* **452**, 202–205.

Nassar, H., Zyoud, A., El-Hamouz, A., Tanbour, R., Halayqa, N. & Hilal, H. S. 2020 Aqueous nitrate ion adsorption/desorption by olive solid waste-based carbon activated using $ZnCl_2$. *Sustainable Chemistry and Pharmacy* **18**, 100335.

Ogata, F., Nagai, N., Kariya, Y., Nagahashi, E., Kobayashi, Y., Nakamura, T. & Kawasaki, N. 2018 Adsorption of nitrite and nitrate ions from an aqueous solution by Fe–Mg-type hydrotalcites at different molar ratios. *Chemical and Pharmaceutical Bulletin* **66**, 458–465.

Pandi, K. & Viswanathan, N. 2016 *In situ* fabrication of magnetic iron oxide over nano-hydroxyapatite gelatin eco-polymeric composite for defluoridation studies. *Journal of Chemical & Engineering* **61**, 571–578.

Rodrigues, E., Almeida, O., Brasil, H., Moraes, D. & dos Reis, M. A. L. 2019 Adsorption of chromium (VI) on hydrotalcite–hydroxyapatite material doped with carbon nanotubes: equilibrium, kinetic and thermodynamic study. *Applied Clay Science* **172**, 57–64.

Saiah, F. B. D., Su, B.-L. & Bettahar, N. 2009 Nickel–iron layered double hydroxide (LDH): textural properties upon hydrothermal treatments and application on dye sorption. *Journal of Hazardous Materials* **165**, 206–217.

Saifullah, B. & Hussein, M. Z. B. 2015 Inorganic nanolayers: structure, preparation, and biomedical applications. *International Journal of Nanomedicine* **10**, 5609–5633.

Samatya, S., Kabay, N., Yüksel, Ü., Arda, M. & Yüksel, M. 2006 Removal of nitrate from aqueous solution by nitrate selective ion exchange resins. *Reactive & Functional Polymers* **66**, 1206–1214.

Shahwan, T. 2021 Critical insights into the limitations and interpretations of the determination of ΔG^o, ΔH^o, and ΔS^o of sorption of aqueous pollutants on different sorbents. *Colloid and Interface Science Communications* **41**, 100369.

Shen, J., Zhou, Y., Li, S., Gu, P. & Xue, G. 2019 Hydrogel-coated Fe_3O_4 nanoparticles as an efficient heterogeneous Fenton catalyst for degradation of phenol. *Journal of Materials Science* **54**, 10684–10694.

Shi, Y., Li, J., Wan, D., Huang, J. & Liu, Y. 2020 Peroxymonosulfate-enhanced photocatalysis by carbonyl-modified g-C_3N_4 for effective degradation of the tetracycline hydrochloride. *Science of the Total Environment* **749**, 142313.

Song, W., Gao, B., Xu, X., Wang, F., Xue, N., Sun, S., Song, W. & Jia, R. 2016 Adsorption of nitrate from aqueous solution by magnetic amine-crosslinked biopolymer based corn stalk and its chemical regeneration property. *Journal of Hazardous Materials* **304**, 280–290.

Sun, X. F., Imai, T., Sekine, M., Higuchi, T., Yamamoto, K. & Akagi, K. 2013 Adsorption of phosphate by calcinated Mg-Fe layered double hydroxide. *Journal of Water & Environment Technology* **11**, 111–120.

Toledo, T. V., Bellato, C. R., Rosário, R. H. & Marques Neto, J. O. 2010 Adsorption of arsenic(V) by the magnetic hydrotalcite–iron oxide composite. *Química Nova* **34**, 561–567.

Wan, D., Liu, H., Liu, R., Qu, J., Li, S. & Zhang, J. 2012 Adsorption of nitrate and nitrite from aqueous solution onto calcined (Mg–Al) hydrotalcite of different Mg/Al ratio. *Chemical Engineering Journal* **195–196**, 241–247.

Wang, M., Guo, P. Y., Zhang, Y., Lv, C. M., Liu, T. Y., Chai, T. Y., Xie, Y. H., Wang, Y. Z. & Zhu, T. 2018 Synthesis of hollow lantern-like Eu(III)-doped g-C_3N_4 with enhanced visible light photocatalytic performance for organic degradation. *Journal of Hazardous Materials* **349**, 224–233.

Wiercik, P., Domańska, M. & Konieczny, T. 2020 Nitrogen recovery from reject water by the production of nitrite concentrate via nitritation, membrane processes and ion exchange. *Desalination and Water Treatment* **197**, 90–100.

Xia, N. N., Zhang, H. Y., Hu, Z. H., Kong, F. & He, F. 2020 A functionalized bio-based material with abundant mesopores and catechol groups for efficient removal of boron. *Chemosphere* **263**, 128202.

Xu, L. & Wang, J. 2012 Fenton-like degradation of 2,4-dichlorophenol using Fe_3O_4 magnetic nanoparticles. *Applied Catalysis B: Environmental* **123–124**, 117–126.

Yan, L.-g., Yang, K., Shan, R.-r., Yu, H.-q. & Du, B. 2015 Calcined ZnAl- and Fe_3O_4/ZnAl-layered double hydroxides for efficient removal of Cr(VI) from aqueous solution. *RSC Advances* **5**, 96495–96503.

Yang, Y., Gao, N., Chu, W., Zhang, Y. & Ma, Y. 2012 Adsorption of perchlorate from aqueous solution by the calcination product of Mg/(Al–Fe) hydrotalcite-like compounds. *Journal of Hazardous Materials* **209–210**, 318–325.

Zeng, D., Liang, K., Guo, F., Wu, Y. & Wu, G. 2020 Denitrification performance and microbial community under salinity and MIT stresses for reverse osmosis concentrate treatment. *Separation and Purification Technology* **242**, 116799.

Zhang, X. F., Wang, J., Li, R. M., Dai, Q. H., Gao, R., Liu, Q. & Zhang, M. L. 2013 Preparation of Fe_3O_4@C@layered double hydroxide composite for magnetic separation of uranium. *Industrial & Engineering Chemistry Research* **52**, 10152–10159.

Received 28 August 2020; accepted in revised form 28 May 2021. Available online 15 June 2021